

Fast-rotating bars in the Λ CDM cosmological paradigm

F. Fragkoudi^{1,2*}, R. J. J. Grand², R. Pakmor², V. Springel², S. D. M. White², F. Marinacci³, F. A. Gomez^{4,5}, and J. F. Navarro⁶

¹ European Southern Observatory, Karl-Schwarzschild-Str. 2, 85748 Garching-bei-München, Germany
e-mail: francesca.fragkoudi@eso.org

² Max-Planck-Institut für Astrophysik, Karl-Schwarzschild-Str. 1, 85748 Garching, Germany

³ Department of Physics and Astronomy, University of Bologna, via Gobetti 93/2, I-40129 Bologna, Italy

⁴ Instituto de Investigación Multidisciplinar en Ciencia y Tecnología, Universidad de La Serena, Raul Bitrán 1305, La Serena, Chile

⁵ Departamento de Astronomía, Universidad de La Serena, Av. Juan Cisternas 1200 Norte, La Serena, Chile

⁶ Department of Physics and Astronomy, University of Victoria, Victoria, BC, V8P 5C2, Canada

Received xx xx; Accepted xx xx

ABSTRACT

The pattern speed with which galactic bars rotate is intimately linked to the amount of dark matter in the inner regions of their host galaxies. In particular, dark matter haloes act to slow down bars via torques exerted through dynamical friction. Observational studies of barred galaxies tend to find that bars rotate fast, while hydrodynamical cosmological simulations of galaxy formation and evolution in the Λ CDM framework have previously found that bars slow down excessively. This has led to a growing tension between fast bars and the Λ CDM cosmological paradigm. In this study we revisit this issue, using the Auriga suite of high resolution, magneto-hydrodynamical cosmological zoom-in simulations of galaxy formation and evolution in the Λ CDM framework, finding that bars remain fast down to $z = 0$. In Auriga, bars form in galaxies that have higher stellar-to-dark matter ratios and are more baryon-dominated than in previous cosmological simulations; this suggests that in order for bars to remain fast, massive spiral galaxies must lie above the commonly used abundance matching relation. While this work may resolve the aforementioned tension between fast bars and Λ CDM, it accentuates the recently reported discrepancy between the dynamically inferred stellar-to-dark matter ratios of massive spirals and those inferred from abundance matching. Our results highlight the potential of using bar dynamics to constrain models of galaxy formation and evolution.

Key words. giant planet formation – κ -mechanism – stability of gas spheres

1. Introduction

Bars are common structures in spiral galaxies in the local Universe (Eskridge et al. 2000; Menéndez-Delmestre et al. 2007) and are able to redistribute angular momentum (Lynden-Bell & Kalnajs 1972) from the inner regions of the disc to the outer disc and dark matter halo, with the distribution function of the galaxy determining the amount of material which is available to ‘absorb’ and ‘emit’ this angular momentum (Athanasoula 2003). The distribution of dark matter in the inner regions of haloes is therefore one of the main factors driving the formation and evolution of bars themselves (Debattista & Sellwood 2000), while other important factors include the velocity dispersion of the disc and halo, the central mass concentration and the gas fraction in the disc (Ostriker & Peebles 1973; Combes & Sanders 1981; Athanasoula et al. 2013).

The inner regions of stellar discs lose angular momentum via the bar, by trapping stars onto elongated orbits – and therefore growing in mass and length over time (Athanasoula 2003) – and through dynamical friction with the dark matter halo (Tremaine & Weinberg 1984b; Weinberg 1985). Dynamical friction can act to slow down the angular rotation speed of the bar (Tremaine & Weinberg 1984b), commonly referred to as the bar pattern speed, Ω_p , without increasing the length of the bar, R_{bar} (Debattista & Sellwood 2000). When bars slow down, the corotation radius, R_{CR} – the radius at which stars on near circular orbits

move around the galaxy with the same angular frequency as the bar – increases. As a result, the corotation radius normalised by the bar length, $\mathcal{R} = R_{\text{CR}}/R_{\text{bar}}$, can shed light on how much dynamical friction the halo exerts on the bar, and therefore on the amount of dark matter in the inner galaxy. As is common in the literature, in what follows we will refer to bars with $\mathcal{R} < 1.4$ and $\mathcal{R} > 1.4$ as “fast” and “slow” respectively (Debattista & Sellwood 2000).

Numerous observational efforts have been made to measure the pattern speed of bars, finding that bars tend to rotate fast, i.e. have $\mathcal{R} < 1.4$ (Corsini 2011; Aguerri et al. 2015; Guo et al. 2019). This suggests that dark matter haloes do not exert much dynamical friction on bars, and are therefore likely subdominant in the central regions of galaxies. However, uncertainties in obtaining the mass-to-light ratio (M/L) of stellar discs make determining the baryon-to-dark matter ratio in the inner regions of galaxies difficult. Dynamical studies of massive spiral galaxies in the local Universe tend to find that these are baryon-dominated in their central regions (Weiner et al. 2001; Kranz et al. 2003; Bovy & Rix 2013; Fragkoudi et al. 2017). This is also found by studies which use the less uncertain M/L obtained from stellar population models in the near-infrared (Lelli et al. 2016). On the other hand, studies such as the DiskMass Survey point to contradictory results, suggesting that dark matter haloes dominate in the central regions of spiral galaxies (Bershady et al. 2011). Therefore, whether or not spiral galaxies are baryon-dominated in their central regions, is still under debate.

* e-mail: francesca.fragkoudi@eso.org

On the other hand, advances in numerical and physical implementations have led to drastic improvements in hydrodynamical cosmological simulations, which are now able to routinely form spiral galaxies with extended discs (Agertz et al. 2011; Vogelsberger et al. 2014; Schaye et al. 2015; Grand et al. 2017). However, the relative contribution of baryonic and dark matter in the inner regions of galaxies in Λ CDM is an ongoing topic of debate, as baryonic processes play an important role in reshaping the inner profiles of dark matter haloes and in setting the baryon-to-dark matter ratio in the central regions (Moore 1994; Pontzen & Governato 2012; Lovell et al. 2018). Studying the dynamics of barred galaxies in cosmological simulations provides a powerful tool for constraining the relative amount of baryons and dark matter in the inner regions.

There have been a handful of studies which have explored the properties of bars in the full Λ CDM cosmological context to date (e.g. Kraljic et al. 2012; Scannapieco & Athanassoula 2012; Zana et al. 2018; Rosas-Guevara et al. 2020; Blázquez-Calero et al. 2020). However, few of these have explored their pattern speeds, and only two explore this in a large sample of galaxies (Algorry et al. 2017; Peschken & Łokas 2019), using the EAGLE (Schaye et al. 2015) and Illustris (Vogelsberger et al. 2014) simulations. These studies found that by $z = 0$, bars have slowed down excessively, making them incompatible with observations. This has resulted in a growing tension between Λ CDM cosmological simulations and fast bars, raising the question, are fast bars incompatible with the Λ CDM framework?

Here we revisit the problem of the slow-down of bars in the Λ CDM cosmological context, using the Auriga simulations, a suite of state-of-the-art high-resolution magneto-hydrodynamical cosmological zoom-in simulations of the formation of Milky Way-mass galaxies. In Section 2 we briefly describe the sample of simulations used in this study and present the pattern speed of bars in Auriga. In Section 3 we compare our results to previous results in the literature, and discuss differences in the simulations that can give rise to the different dynamical behaviour. In Section 4 we discuss some of the implications of our findings and conclude.

2. Fast-rotating bars in the Auriga Simulations

2.1. The Auriga Simulations

The Auriga simulations (Grand et al. 2017) are a suite of 30 magneto-hydrodynamical cosmological zoom simulations of haloes with masses in the range of $1 \times 10^{12} - 2 \times 10^{12} M_{\odot}$ which run from redshift $z = 127$ to $z = 0$ with cosmological parameters $\Omega_m = 0.307$, $\Omega_b = 0.048$, and a Hubble constant of $H_0 = 67.77 \text{ km s}^{-1} \text{ Mpc}^{-1}$ (Planck Collaboration et al. 2014); unless otherwise stated we use these parameters throughout the paper. The simulations are performed with the magneto-hydrodynamic code AREPO (Springel 2010; Pakmor et al. 2016), with a comprehensive galaxy formation model (Vogelsberger et al. 2013; Marinacci et al. 2014; Grand et al. 2016) and form star-forming disc galaxies with flat rotation curves that reproduce a range of observed scaling relations such as the Tully-Fisher relation (Grand et al. 2017) and the size-mass relation of HI gas discs (Marinacci et al. 2017). They form structures such as bars and boxy/peanuts which have properties compatible with those of observed bars (Blázquez-Calero et al. 2020; Fragkoudi et al. 2020) and mainly consist of so-called pseudo-bulges (Gargiulo et al. 2019). For more details we refer the reader to the aforementioned papers and references therein.

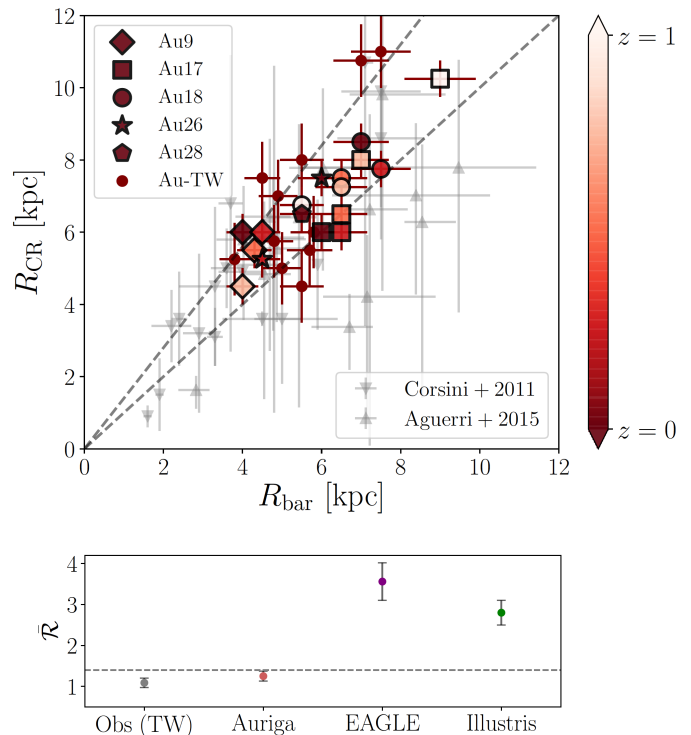


Fig. 1. Bar corotation radius vs bar length for Auriga galaxies: *Top panel:* Corotation radius as a function of bar length for the barred Auriga galaxies, denoted by the symbols in the figure legend. The colour-coding corresponds to measurements at different redshifts, while for the galaxies for which we use the TW method (Au-TW) we estimate the pattern speed at $z = 0$. These are compared to data from Corsini (2011) and Aguerri et al. (2015) (grey points); the error bars indicate the 1σ uncertainties. The lower and upper dashed grey lines indicate $R = 1$ and $R = 1.4$ respectively. Bars in Auriga are fast across all redshifts. *Bottom panel:* We show the mean R for the aforementioned observations, for barred galaxies in Auriga, and for the EAGLE and Illustris barred galaxies from Algorry et al. (2017) and Peschken et al. (2019) at $z = 0$. The error bars indicate the 2σ error on the mean. The dashed line indicates $R = 1.4$, below which bars are considered fast. Bars in the Auriga simulations are fast, compatible with observations, while bars in EAGLE and Illustris are excessively slow at $z = 0$.

In this study our ‘barred sample’ includes all the Auriga galaxies with bar strength $A_2 > 0.2$, at $z = 0$. This excludes five Auriga galaxies which are undergoing an interaction at $z = 0$ (Au1, Au11, Au20, Au25 and Au30). For these galaxies the pattern speed cannot be reliably measured using the Tremaine-Weinberg method, for which the continuity equation must hold. We therefore have 16 Auriga galaxies in our barred sample. Five of these haloes (Au9, Au17, Au18, Au26 and Au28) are re-runs of the original Auriga haloes with higher cadence outputs (i.e. every 10 Myr), in order to be able to determine the pattern speed from the temporal evolution of the bar and to test our implementation of the Tremaine-Weinberg method (due to the high computational cost we do not re-run all the Auriga galaxies). For the re-runs, the initial conditions of the haloes and the physics implementations are the same as those of the original Auriga haloes. We refer the reader to the Appendix where we describe in detail how we obtain the bar strength, length and pattern speed of our simulated galaxies.

2.2. Dynamically fast bars in Auriga

As mentioned above, while the absolute value of the pattern speed of bars can shed light on the exchange of angular momentum in the galaxy, the parameter used to determine the bar slow-down due to dynamical friction is $\mathcal{R} = R_{\text{CR}}/R_{\text{bar}}$ due to the fact that dynamical friction can act to slow down the bar without a corresponding increase in its length. We plot R_{CR} versus R_{bar} in the top panel of Figure 1 for the barred Auriga galaxies and compare these to observations (Corsini 2011; Aguerri et al. 2015), in which the bar pattern speed is obtained using the Tremaine-Weinberg (TW) method (Tremaine & Weinberg 1984a). The upper and lower solid lines in the figure correspond to $\mathcal{R} = 1.4$ and 1 respectively, which denote the regime in which bars are considered ‘fast’. For the five Auriga galaxies for which we have high cadence outputs we calculate the corotation radius and bar length at redshifts $z = 0, 0.25, 0.5, 0.75, 1$ (provided the bar has already formed by the corresponding redshift), as denoted by the colour-coding of the symbols. We find that when bars in the Auriga galaxies are formed, they have $\mathcal{R} < 1.4$, i.e. they are dynamically fast, and that they remain so throughout their evolution, i.e. the Auriga bars are fast within the uncertainties at $z = 0$.

3. Comparison with previous results on the pattern speed of bars in cosmological simulations

In the bottom panel of Figure 1 we show the mean and 2σ error on the mean of \mathcal{R} , for barred galaxies in the Auriga simulations, for the above-mentioned observations, as well as for the barred galaxies studied previously in the Λ CDM framework (Algorry et al. 2017; Peschken & Łokas 2019), i.e. in the EAGLE and Illustris simulations. Bars in EAGLE and Illustris tend to have $\mathcal{R} > 2.5$, in tension with observations. Bars in Auriga have $\mathcal{R} < 1.4$, thus demonstrating that bars can remain dynamically fast in cosmological simulations within the Λ CDM paradigm, and resolving the previously reported tension between observed fast bars and Λ CDM.

A natural question to ask is ‘what gives rise to the different behaviour of \mathcal{R} in the different simulations?’ As mentioned above, \mathcal{R} depends on the amount of dynamical friction exerted by the halo on the disc, which in turn depends strongly on the amount of dark matter present in the central region of the halo as compared to the disc mass. The subgrid physics modelling employed in cosmological simulations can therefore play a critical role in determining the bar properties, and more crucially, its slowdown rate, as it sets the disc-to-halo mass ratio in the central regions of galaxies. On the other hand, the lower numerical resolution of the EAGLE and Illustris simulations as compared to Auriga might also have an effect on \mathcal{R} .

3.1. Resolution

Low numerical resolution has been extensively discussed in the literature as a parameter which could affect the evolution of bars and the exchange of angular momentum at resonances, with different studies often reaching contradictory conclusions (Weinberg 1998; Weinberg & Katz 2002; Valenzuela & Klypin 2003; Sellwood 2006, 2008).

In order to test the effect of resolution in our models, and to explore whether it could be the primary reason for why previous studies using the EAGLE and Illustris cosmological simulations found large values of \mathcal{R} , we carry out a resolution test. We reran two of our Auriga haloes (Au17 and Au18) with $8\times$ lower mass resolution, and $2\times$ lower spatial resolution. This leads to a

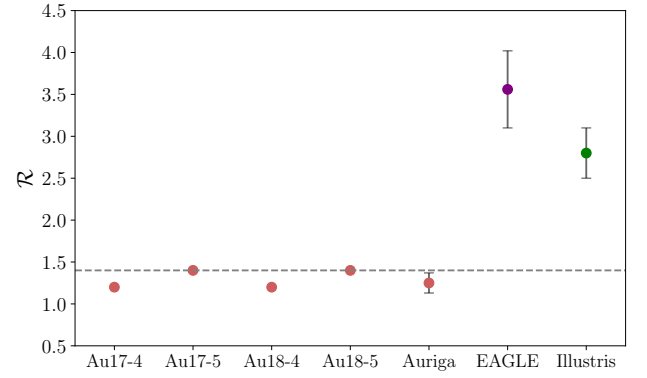


Fig. 2. Resolution test for \mathcal{R} : We show the value of \mathcal{R} for the two lower resolution runs for Au17 and Au18 (Au17-5 and Au18-5) compared to the standard resolution runs used in this paper, Au17-4 and Au18-4. For reference we also show the mean and 2σ error of \mathcal{R} for EAGLE and Illustris.

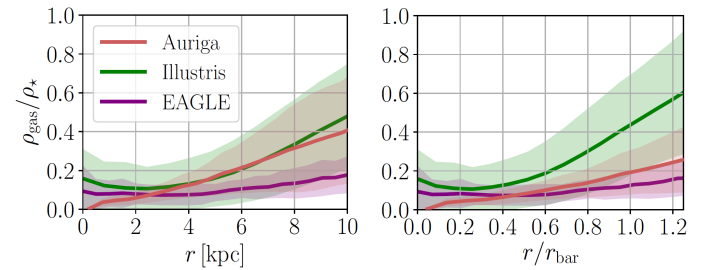


Fig. 3. Gas fraction in the simulations: *Left:* The average gas density over stellar density in the Auriga galaxies as compared to disc galaxies in EAGLE and Illustris. *Right:* As in the left panel, with the radius normalised by the average bar length in each of the simulations.

mass resolution that is closer to – although still slightly higher than – the EAGLE and Illustris resolution. In the low resolution Auriga runs the stellar and dark matter particles have a mass of $4\times 10^5 M_\odot$ and $3.2\times 10^6 M_\odot$ respectively, while in EAGLE (Illustris) the stellar mass is $1.8\times 10^6 M_\odot$ ($1.3\times 10^6 M_\odot$) and the dark matter particle mass is $9.7\times 10^6 M_\odot$ ($6.3\times 10^6 M_\odot$). If resolution is the major contributor to the high values of \mathcal{R} in previous studies we expect to see a significant effect on \mathcal{R} when decreasing the resolution to be close to that of EAGLE and Illustris.

In Figure 2 we show the \mathcal{R} values for the level 4 (high resolution) and level 5 (low resolution) runs for Au17 and Au18. We find that \mathcal{R} has a slight increase of $\sim 15\%$ in the low resolution runs. However, the increase is within the 2σ error of the mean \mathcal{R} values for the high resolution barred galaxies explored in this study (indicated by the error bar for the point denoted ‘Auriga’). Therefore the small increase in \mathcal{R} for the low resolution Auriga runs (15%) does not appear to be sufficient to explain the much higher values found in the EAGLE and Illustris simulations¹. These considerations suggest that resolution is likely not the main culprit for the high \mathcal{R} values found in previous simulations such as EAGLE and Illustris.

3.2. Gas fraction

The fraction of gas within discs, and in particular within the bar radius, can play a role in both the formation and strength of bars.

¹ It is also worth noting that other high-resolution zoom simulations in the literature (e.g. Zana et al. 2018) – which have studied the pattern speed of bars – also find bars with $\mathcal{R} > 1.4$ at $z = 0$.

It has also been suggested that gas can play a role in maintaining fast bars (Athanasoula 2014), although the topic has given rise to considerable debate (e.g. Bournaud et al. 2005; Berentzen et al. 2007; Athanasoula 2014; Sellwood & Debattista 2014 and references therein). In Figure 3 we explore the gas content of disc galaxies in Auriga, EAGLE and Illustris. Auriga and Illustris have similar gas fractions within 10 kpc, while EAGLE has lower gas fractions, which could possibly contribute to the slower bars in EAGLE as compared to Auriga. However, when the radius is normalised by the average bar length in each simulation, we find that, within one bar radius, Auriga galaxies have in fact similar gas fractions to EAGLE, and lower gas fractions than Illustris. Therefore, while the gas fraction might contribute to the differences in pattern speed between the different simulations, it is likely not the main culprit for allowing Auriga to maintain fast bars.

3.3. Baryon-dominance

We therefore turn our attention to the relative amount of the stellar component compared to dark matter in the Auriga simulations. We explore this in Figure 4 and compare Auriga to the EAGLE and Illustris cosmological simulations. In the left panel we plot the average and 1σ relation for the stellar mass as a function of the dark matter halo mass (M_\star vs M_h) for the Auriga galaxies (red), as well as for the Illustris and EAGLE discs (green and purple respectively). We compare these to the commonly used abundance matching relation (Moster et al. 2018; dashed blue line), which is obtained by matching the observed stellar mass function to the halo mass function in cosmological simulations. Auriga galaxies are offset from the relation, and lie above both the EAGLE and Illustris discs, i.e. they are globally more baryon-dominated. In the middle panel of Figure 4 we plot the efficiency with which – given a universal baryon-to-dark matter ratio $f_b = \Omega_b/\Omega_c$ – galaxies convert their gas into stars, i.e. $f_\star = M_\star/(f_b M_h)$, as a function of stellar mass. This is shown for the Auriga, EAGLE and Illustris simulations, for both the entire disc sample (circles) and for the barred galaxies (squares). The Auriga galaxies are offset from the relation predicted by abundance matching – by more than 2σ at $M_\star = 9 \times 10^{10} M_\odot$. They also lie above both the EAGLE and Illustris galaxies, and thus have higher global stellar-to-dark matter ratios for a given stellar mass at $z = 0$. Recent work by Posti et al. (2019) explored galaxies in the SPARC sample (Lelli et al. 2016), finding that massive spirals lie above the relation for f_\star derived from abundance matching, which implies that massive spirals are overly efficient at converting gas to stars (the so-called this the ‘failed feedback problem’). A subsequent study by Marasco et al. (2020) found that massive spirals in SPARC are more baryon-dominated than spiral galaxies in cosmological simulations such as EAGLE and IllustrisTNG100. Interestingly, the Auriga galaxies follow a similar trend as the high mass spiral galaxies in the SPARC sample, which are denoted by the grey symbols.

What causes Auriga to be more baryon-dominated than the EAGLE and Illustris simulations is the complex interplay of the subgrid implementations of the various physical processes occurring in the simulations. A full exploration of these is beyond the scope of this paper, but here we outline a few likely important differences and refer the reader to the papers describing the simulations for more details (Schaye et al. 2015; Vogelsberger et al. 2014; Grand et al. 2017). The wind supernova feedback model in Auriga has significant differences from its predecessor, Illustris, in both its parametrization and its implementation, e.g. the winds are isotropic in Auriga vs bipolar in Illustris. This

might lead to the winds being more effective at higher redshifts in Auriga where galaxies are irregular. On the other hand, EAGLE employs a thermal feedback prescription which is more ‘bursty’, heating particles stochastically to sufficiently high temperatures to avoid catastrophic cooling, which is likely more effective at removing baryons from the central regions of galaxies. The prescription of AGN feedback in Auriga is ‘smoother’ than that in Illustris and EAGLE: in Auriga the ‘bubble’ radio-mode feedback provides a more gentle and distributed heating of the circum-galactic medium than in Illustris, in which a smaller number of very energetic bubbles were able to blow out all the gas from the halo; in EAGLE there is only one mode of AGN feedback in which thermal energy is injected stochastically by heating particles around the black hole to very high temperatures. Furthermore, Auriga includes magnetic fields, in contrast to both EAGLE and Illustris. The differences in these physical modelling assumptions, which combine non-linearly, give rise to discs which are more baryon-dominated in Auriga.

While the $M_\star - M_h$ relation tells us about the global ratio of baryons-to-dark matter, the local distribution of baryons-to-dark matter is more relevant for the dynamics of disc galaxies and for the bar instability. We show this in the right panel of Figure 4, where we plot V_\star/V_{tot} , i.e. the ratio of the stellar component to the total rotation curve, as a function of radius for disc galaxies in Auriga, Illustris and EAGLE (in the mass range $3 \times 10^{10} < M_\star/M_\odot < 10^{11}$). This reveals how ‘maximal’ or baryon-dominated a galaxy is, which in turn will partially determine whether the disc is able to form a bar that remains fast. Historically, this has been calculated at a given radius to determine ‘maximality’, such as at 2.2 disc scalelengths. We find that the Auriga barred galaxies are overall more baryon-dominated than EAGLE and Illustris. In Figure C.1 we explore this trend also at redshift $z = 0.5$ and find that Auriga galaxies are already more baryon-dominated at higher redshifts.

4. Discussion & Conclusions

These considerations provide us with an explanation for why bars in previous cosmological simulations have tended to slow down so dramatically by $z = 0$: their host galaxies are embedded in dominant dark matter haloes – both locally and globally – and thus their bars suffer more dynamical friction. Disc galaxies in the Auriga simulations, on the other hand, are more baryon-dominated, and thus are able to remain fast for over half the age of the Universe. This alleviates the previously reported tension between fast bars and the Λ CDM cosmological paradigm. However, our findings suggest that in order to reproduce the dynamics of barred galaxies, massive spirals must be baryon-dominated, and should lie $\sim 2\sigma$ above the abundance matching relation. This is consistent with the recently reported findings of Posti et al. (2019) and Marasco et al. (2020), which highlight the tension between the stellar-to-dark matter ratio of high mass spirals obtained dynamically and via abundance matching.

Our results imply that, from a dynamical perspective, cosmological simulations of galaxy formation and evolution can reproduce the properties of observed barred spirals provided they are able to build up more stellar mass in the disc than predicted by abundance matching. This suggests that care is needed to not make the stellar and AGN feedback prescriptions overly effective, as this can lead to lower stellar-to-dark matter ratios in high-mass spirals, which will prevent them from maintaining fast bars within the Λ CDM framework. As bars are present in a significant fraction ($\geq 50\%$) of the population of spiral galaxies in the local Universe (Eskridge et al. 2000; Menéndez-Delmestre

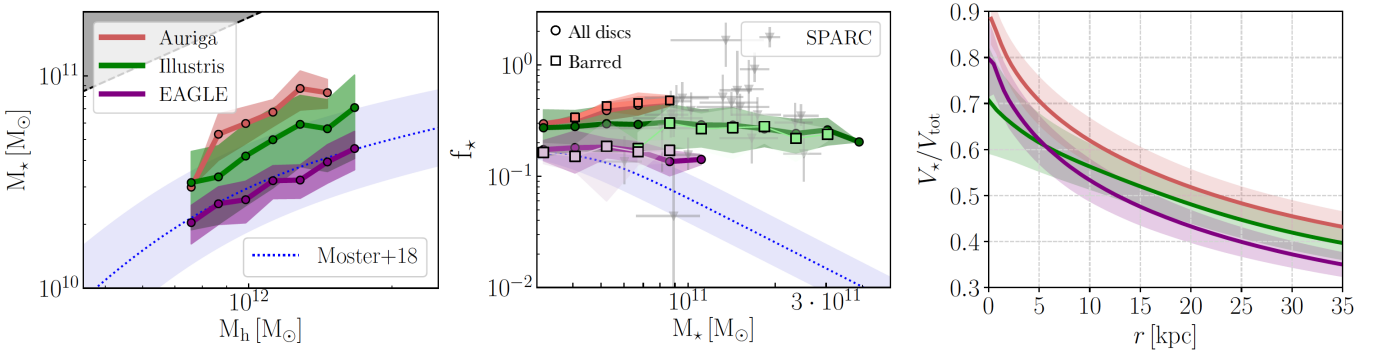


Fig. 4. Global and local stellar-to-dark matter ratios in the Auriga galaxies as compared to EAGLE and Illustris: *Left:* The mean (lines) and 1σ (shaded region) values of the M_* vs M_h of Auriga, EAGLE and Illustris disc galaxies at $z = 0$ compared to the abundance matching relation from Moster et al. (2018). *Middle:* The efficiency with which gas is turned into stars, i.e. $f_* = \frac{M_*}{f_b M_h}$ as a function of stellar mass for the Auriga, EAGLE and Illustris galaxies, compared to the relation from abundance matching. The mean and 1σ values for disc (barred) galaxies are shown with the circles/thick lines (squares/thin lines) and shaded region respectively. For comparison we also show the high mass disc galaxies from the SPARC sample explored in Marasco et al. (2020), where the error bars denote 16th-84th percentile uncertainties. *Right:* The local baryon dominance, V_*/V_{tot} as a function of radius, of Auriga, EAGLE and Illustris disc galaxies in the mass range $3 \times 10^{10} < M_*/M_\odot < 10^{11}$.

et al. 2007), this effect is likely to considerably increase the expected scatter around the abundance matching relation, particularly for spirals at the high-mass end, where bars are more numerous (Masters et al. 2012; Gavazzi et al. 2015). In order to determine whether these results have repercussions on the expected value of the abundance matching relation or simply on its scatter, will depend on the relation followed by the global population of galaxies at this mass range, including early type galaxies, which are abundant at these masses. In terms of the implications for lower mass galaxies, there is still considerable debate in the observational community with regards to the frequency of bars in lower mass spirals (Nair & Abraham 2010; Erwin 2018), and as such, an exploration of the properties of lower mass barred spirals in cosmological simulations is timely.

Our results highlight the importance of taking into account the dynamics of barred spiral galaxies when constraining models of galaxy formation and evolution.

Acknowledgements. FF thanks Lorenzo Posti, Ben Moster and Cilia Damiani for useful discussions and Nicolas Peschken for providing the halo IDs of barred galaxies in the Illustris simulation.

References

Agertz, O., Teyssier, R., & Moore, B. 2011, *MNRAS*, 410, 1391
 Aguerri, J. A. L., Méndez-Abreu, J., Falcón-Barroso, J., et al. 2015, *A&A*, 576, A102
 Algorry, D. G., Navarro, J. F., Abadi, M. G., et al. 2017, *MNRAS*, 469, 1054
 Athanassoula, E. 2003, *MNRAS*, 341, 1179
 Athanassoula, E. 2014, *MNRAS*, 438, L81
 Athanassoula, E., Machado, R. E. G., & Rodionov, S. A. 2013, *MNRAS*, 429, 1949
 Berentzen, I., Shlosman, I., Martínez-Valpuesta, I., & Heller, C. H. 2007, *ApJ*, 666, 189
 Bershadsky, M. A., Martinsson, T. P. K., Verheijen, M. A. W., et al. 2011, *ApJ*, 739, L47
 Binney, J. & Tremaine, S. 2008, *Galactic Dynamics*, 2nd edn. (Princeton University Press), 920
 Blázquez-Calero, G., Florido, E., Pérez, I., et al. 2020, *MNRAS*, 491, 1800
 Bournaud, F., Combes, F., & Semelin, B. 2005, *MNRAS*, 364, L18
 Bovy, J. & Rix, H.-W. 2013, *ApJ*, 779, 115
 Combes, F. & Sanders, R. H. 1981, *A&A*, 96, 164
 Corsini, E. M. 2011, *Memorie della Società Astronomica Italiana Supplementi*, 18, 23
 Debattista, V. P. & Sellwood, J. A. 2000, *ApJ*, 543, 704
 Erwin, P. 2005, *MNRAS*, 364, 283
 Erwin, P. 2018, *MNRAS*, 474, 5372
 Eskridge, P. B. et al. 2000, *AJ*, 119, 536

Fragkoudi, F., Athanassoula, E., & Bosma, A. 2017, *MNRAS*, 466, 474
 Fragkoudi, F., Grand, R. J. J., Pakmor, R., et al. 2020, *MNRAS*, 494, 5936
 Gargiulo, I. D., Monachesi, A., Gómez, F. A., et al. 2019, *arXiv e-prints*, arXiv:1907.02082
 Gavazzi, G., Consolandi, G., Dotti, M., et al. 2015, *A&A*, 580, A116
 Grand, R. J. J., Bustamante, S., Gómez, F. A., et al. 2017, *ArXiv e-prints* [arXiv:1708.07834]
 Grand, R. J. J., Springel, V., Gómez, F. A., et al. 2016, *MNRAS*, 459, 199
 Guo, R., Mao, S., Athanassoula, E., et al. 2019, *MNRAS*, 482, 1733
 Kraljic, K., Bournaud, F., & Martig, M. 2012, *ApJ*, 757, 60
 Kranz, T., Slyz, A., & Rix, H.-W. 2003, *ApJ*, 586, 143
 Lelli, F., McGaugh, S. S., & Schombert, J. M. 2016, *AJ*, 152, 157
 Lovell, M. R., Pillepich, A., Genel, S., et al. 2018, *MNRAS*, 481, 1950
 Lynden-Bell, D. & Kalnajs, A. J. 1972, *MNRAS*, 157, 1
 Marasco, A., Posti, L., Oman, K., et al. 2020, *arXiv e-prints*, arXiv:2005.01724
 Marinacci, F., Grand, R. J. J., Pakmor, R., et al. 2017, *MNRAS*, 466, 3859
 Marinacci, F., Pakmor, R., & Springel, V. 2014, *Monthly Notices of the Royal Astronomical Society*, 437, 1750
 Masters, K. L., Nichol, R. C., Haynes, M. P., et al. 2012, *MNRAS*, 424, 2180
 McAlpine, S., Helly, J. C., Schaller, M., et al. 2016, *Astronomy and Computing*, 15, 72
 Menéndez-Delmestre, K., Sheth, K., Schinnerer, E., Jarrett, T. H., & Scoville, N. Z. 2007, *ApJ*, 657, 790
 Moore, B. 1994, *Nature*, 370, 629
 Moster, B. P., Naab, T., & White, S. D. M. 2018, *MNRAS*, 477, 1822
 Nair, P. B. & Abraham, R. G. 2010, *ApJ*, 714, L260
 Nelson, D., Pillepich, A., Genel, S., et al. 2015, *Astronomy and Computing*, 13, 12
 Ostriker, J. P. & Peebles, P. J. E. 1973, *ApJ*, 186, 467
 Pakmor, R., Springel, V., Bauer, A., et al. 2016, *MNRAS*, 455, 1134
 Peschken, N. & Łokas, E. L. 2019, *MNRAS*, 483, 2721
 Planck Collaboration, Ade, P. A. R., Aghanim, N., et al. 2014, *A&A*, 571, A16
 Pontzen, A. & Governato, F. 2012, *MNRAS*, 421, 3464
 Posti, L., Fraternali, F., & Marasco, A. 2019, *A&A*, 626, A56
 Rosas-Guevara, Y., Bonoli, S., Dotti, M., et al. 2020, *MNRAS*, 491, 2547
 Scannapieco, C. & Athanassoula, E. 2012, *MNRAS*, 425, L10
 Schaye, J., Crain, R. A., Bower, R. G., et al. 2015, *MNRAS*, 446, 521
 Sellwood, J. A. 2006, *ApJ*, 637, 567
 Sellwood, J. A. 2008, *ApJ*, 679, 379
 Sellwood, J. A. & Debattista, V. P. 2014, *arXiv e-prints*, arXiv:1410.0834
 Springel, V. 2010, *Monthly Notices of the Royal Astronomical Society*, 401, 791
 The EAGLE team. 2017, *arXiv e-prints*, arXiv:1706.09899
 Tremaine, S. & Weinberg, M. D. 1984a, *ApJ*, 282, L5
 Tremaine, S. & Weinberg, M. D. 1984b, *MNRAS*, 209, 729
 Valenzuela, O. & Klypin, A. 2003, *MNRAS*, 345, 406
 Vogelsberger, M., Genel, S., Sijacki, D., et al. 2013, *Monthly Notices of the Royal Astronomical Society*, 436, 3031
 Vogelsberger, M., Genel, S., Springel, V., et al. 2014, *Nature*, 509, 177
 Weinberg, M. D. 1985, *MNRAS*, 213, 451
 Weinberg, M. D. 1998, *MNRAS*, 297, 101
 Weinberg, M. D. & Katz, N. 2002, *ApJ*, 580, 627
 Weiner, B. J., Sellwood, J. A., & Williams, T. B. 2001, *ApJ*, 546, 931
 Zana, T., Dotti, M., Capelo, P. R., et al. 2018, *MNRAS*, 473, 2608

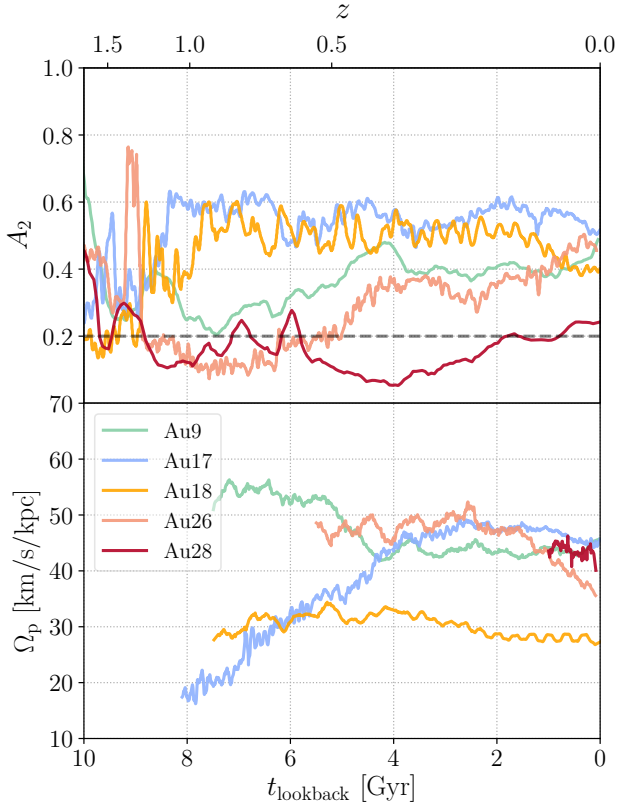


Fig. A.1. Bar properties as a function of time: *Top panel:* Bar strength for the five Auriga galaxies for which we have high cadence outputs as a function of lookback time. The horizontal dashed line indicates $A_2 = 0.2$ above which we consider the bar to have formed. *Bottom panel:* Bar pattern speed for these galaxies, once the bar is formed, as a function of lookback time.

Appendix A: Bar strength and pattern speed

We define the bar strength as the maximum amplitude of the normalised $m = 2$ Fourier mode of the surface density. We select the stellar particles in the disc (i.e. with $|z| < 1$ kpc) in annuli of width 0.5 kpc to calculate,

$$a_m(R) = \sum_{i=0}^N m_i \cos(m\theta_i), \quad m = 0, 1, 2, \dots, \quad (\text{A.1})$$

$$b_m(R) = \sum_{i=0}^N m_i \sin(m\theta_i), \quad m = 0, 1, 2, \dots \quad (\text{A.2})$$

where m_i is the mass of particle i , R is the cylindrical radius, N is the total number of particles in that annulus and θ is the azimuthal angle. To obtain a single value for the bar strength at each time-step, we take the maximum value of the normalised $m = 2$ component,

$$A_2 = \max \left(\frac{\sqrt{a_2^2(R) + b_2^2(R)}}{a_0(R)} \right) \quad (\text{A.3})$$

in radius.

We also carry out visual inspections of the snapshots in order to ensure that the $m = 2$ mode is due to the bar, and not some

other spurious short-lived effect. For example, at high redshifts – when mergers are frequent – short-lived $m = 2$ modes can appear due to the centre of mass of the merging system not being at the centre of the disc (e.g. in the final stages of a merger). This would therefore lead our algorithm to detect a spurious and short-lived $m = 2$ mode, which is however not related to a bar mode in the disc. However we note that such spurious and short-lived spikes in $m = 2$ are essentially only found at high redshifts (see e.g. the large peak in $m = 2$ for Au26 at ~ 9 Gyr in Figure A.1).

For the five galaxies for which we have high cadence outputs the bar pattern speed is obtained by examining the temporal evolution of the bar phase, i.e. by calculating the $m = 2$ phase from the aforementioned Fourier decompositions in each snapshot and as a function of radius as,

$$\theta(R) = 0.5 \arctan \left(\frac{b_2(R)}{a_2(R)} \right). \quad (\text{A.4})$$

The bar pattern speed Ω_p is then calculated as an annular average within the bar radius as,

$$\Omega_p = \frac{\Delta\langle\theta\rangle}{\Delta t}. \quad (\text{A.5})$$

The uncertainty on this value mainly derives from the small oscillations in pattern speed at different snapshots (see for example the bottom panel of Figure A.1), which are typically around ± 2 –3 km/s/kpc. We explored the uncertainty this implies in terms of the corotation radius and found that this translates to $\sim \pm 0.5$ kpc.

In Figure A.1 we show the evolution of the bar strength and pattern speed as a function of lookback time for five of the Auriga galaxies for which we have high cadence outputs. In the top panel of the Figure we show the evolution of the bar strength. Bars form at a range of lookback times in our simulations, with some forming at $z > 1$ (e.g. Au17 and Au18), or as late as 1 Gyr ago (Au28). Bars in Auriga are long-lived structures, i.e. once the bar has formed it does not dissolve. In the bottom panel of Figure A.1 we show the bar pattern speed, Ω_p , for these five barred galaxies as a function of lookback time. Most of the bars have pattern speeds which remain roughly constant or are slightly decreasing (e.g. Au26 after $t_{\text{lookback}} \sim 2$ Gyr). There is also the curious case of Au17, in which the bar pattern speed increases between formation time and until $t_{\text{lookback}} \sim 3$ Gyr due to a resonant interaction with another nearby massive system (a more detailed exploration of this system will be presented elsewhere). The galaxy with the largest decrease in Ω_p , Au26, shows a prototypical example of bar growth in an isolated disc, i.e. while the galaxy evolves in isolation the bar grows gradually stronger over time, while Ω_p decreases. In a number of the other cases shown here, bar formation is triggered after a significant merger, with the disc losing a large fraction of its angular momentum by torques induced during the merger (Fragkoudi et al. 2020), with the bar subsequently not growing much stronger or slower.

For the rest of the Auriga barred sample for which we do not have high cadence outputs we employ the commonly-used Tremaine-Weinberg method (Tremaine & Weinberg 1984a), which uses the continuity equation to estimate the bar pattern speed from a single snapshot at $z = 0$. We tested our method on the five simulations for which we have high cadence outputs – and therefore a reliable estimate for the bar pattern speed – and found that we can typically recover the pattern speed to within ± 5 km/s/kpc. This translates to an error on the corotation radius of $\sim \pm 1$ kpc. These are the uncertainties employed in Figure 1.

Appendix B: Bar length and corotation radius

There is no standard way for estimating the bar length and various methods have been used in observations and simulations – e.g. visual estimation, isophote ellipse fitting, measurements based on Fourier analysis etc. – each with its own advantages and disadvantages (for a discussion of the various methods see Erwin 2005). Here we calculate the bar length using a method commonly used in observations (such as the ones presented in Figure 1), i.e. we fit ellipses to isodensity contours of face-on images of the galaxies. We follow a prescription similar to the one used in Erwin (2005), in which the bar length is defined as the minimum of two ellipse fitting measures: the radius of the first minimum after the maximum of ellipticity, or the radius at which the position angle has an extremum outside the bar. An example of this is shown in the left and middle panels of Figure B.1. If there is no extremum in position angle then we use instead the radius at which the position angle changes by 10 degrees.

To obtain the corotation radius of Auriga barred galaxies we first need to calculate the circular velocity of the galaxy $V_c(r) = r \frac{\partial \Phi}{\partial r}$. We make the simplifying assumption of spherical symmetry, which reduces the circular velocity to $V_c = \sqrt{GM(r)/r}$ where $M(r)$ is the enclosed mass within a sphere of a radius r . This simplification will tend to under-predict the true circular velocity, which will be higher for flatter systems. We tested this by assuming a Miyamoto-Nagai disc (Binney & Tremaine 2008) with realistic flattening of the disc, for which we can calculate V_c analytically. We then calculated the approximate value of V_c using the spherical symmetry assumption. We find that the error in V_c is of the order of $\sim 5 - 10\%$ depending on the flattening of the disc – with the error increasing for thinner discs. For galaxies in our sample which also have a spherical component due the dark matter halo this error will be smaller, roughly of the order of 5%, which is acceptable for the purposes of this study. The angular frequency of stars is then obtained according to $\Omega = V_c/r$ and the epicyclic frequency is calculated as $\kappa = \sqrt{R \frac{d\Omega^2}{dR} + 4\Omega^2}$ (Binney & Tremaine 2008). The corotation radius is the radius at which stars on nearly circular orbits in the disc have the same angular frequency as the bar. We therefore calculate this as the intersection between the Ω curve with the bar pattern speed Ω_p (right panel of Figure B.1).

We note that for the \mathcal{R} values of barred galaxies in EAGLE and Illustris shown in the bottom panel of Figure 1, we use the values reported in Algorry et al. (2017) and Peschken & Łokas (2019) respectively. For the Illustris \mathcal{R} , we divide the value reported in Peschken & Łokas (2019) by 2, since – as stated by the authors – they used a proxy for the bar length which underestimates the true bar length by a factor of ~ 2 .

Appendix C: The abundance matching relation, M_\star and M_h and maximality

In Figures 4 and C.1 we use the abundance matching relation from Moster et al. (2018), employing the values for “All centrals” from their Table 8 and using their derived relation for the scatter in equation 25 (Moster et al. 2018). The values of M_\star and M_h for Auriga, Illustris and EAGLE used in the aforementioned figures are obtained as follows: For Auriga, we calculate M_\star by summing the mass of stellar particles inside 10% of the virial radius of the halo. M_h is the total mass of dark matter particles within the virial radius of the halo. For Illustris, we extract the M_\star within 20 kpc and the total dark matter mass inside the virial radius M_h for disc galaxies using the publicly available Il-

lustris data (Nelson et al. 2015). We use the definition of disc galaxies employed by Peschken & Łokas (2019), i.e. selecting galaxies which have more than 20% of their stellar mass with circularity parameter above 0.7 and with flattened distributions, i.e. which have a flatness ratio (defined by the ratio eigenvalues of the stellar mass tensor) < 0.7 . For the values extracted for the barred Illustris galaxies, we take as barred Illustris galaxies those studied in Peschken & Łokas (2019), in their “total bar” sample (N. Peschken kindly provided us with these galaxy IDs) where barred galaxies are defined as those disc galaxies with $A_2 > 0.15$ with some additional criteria (see Section 2.2 of their paper for more details). For EAGLE, we use the publicly available data from McAlpine et al. (2016) and where relevant the subsequent particle data release (The EAGLE team 2017) to obtain M_\star (stellar mass within 20 kpc) and M_h (dark matter mass within the virial radius) values for disc galaxies in EAGLE, which we define as having stellar velocity rotation-to-dispersion ratios (*RotToDispRatio*), and the stellar disc-to-total ratio from counter rotation (*DiscToTotal*) larger than 1.7 and 0.7, respectively. For the barred galaxies, we use the IDs of the galaxies identified as barred in Algorry et al. (2017).

To explore the local baryon dominance of barred galaxies in Figure 4, we follow the definition of disc maximality used in previous works, i.e. we employ the ratio of the circular velocity due to the stellar component as compared to the total circular velocity. We obtain the stellar and total circular velocities as described in the previous section.

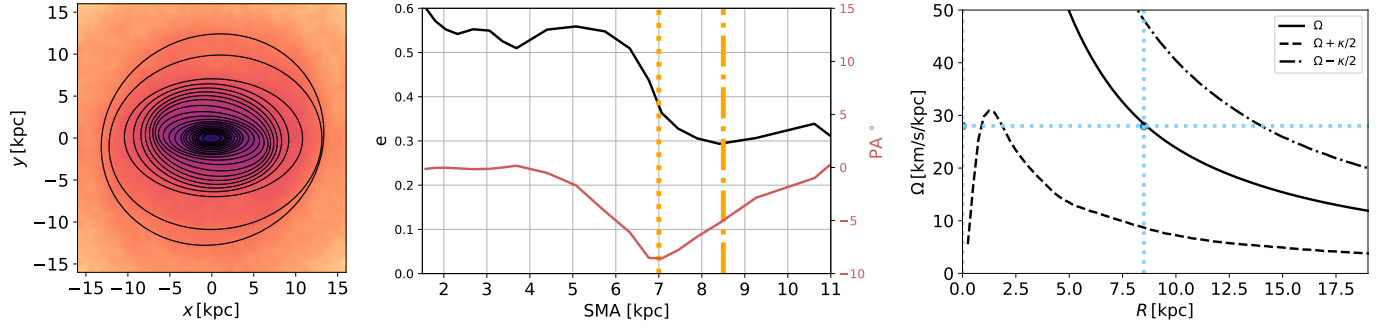


Fig. B.1. Estimating the bar length and corotation radius: *Left panel:* The bar length is estimated by fitting ellipses to iso-density contours. *Middle panel:* Ellipticity and position angle as a function of semi-major axis of the ellipses. The bar length is the minimum of two values: the radius of the first minimum after the ellipticity maximum (dot-dashed orange line) or the radius at which there is the first extremum in position angle outside the bar (dashed line). *Right panel:* The bar corotation radius (marked by the vertical dashed blue line) is the radius at which stars in the disc have the same angular frequency (solid black line) as the bar pattern speed (horizontal dashed blue line). The dashed and dot-dashed lines denote the $\Omega - \kappa/2$ and $\Omega + \kappa/2$ curves for the galaxy.

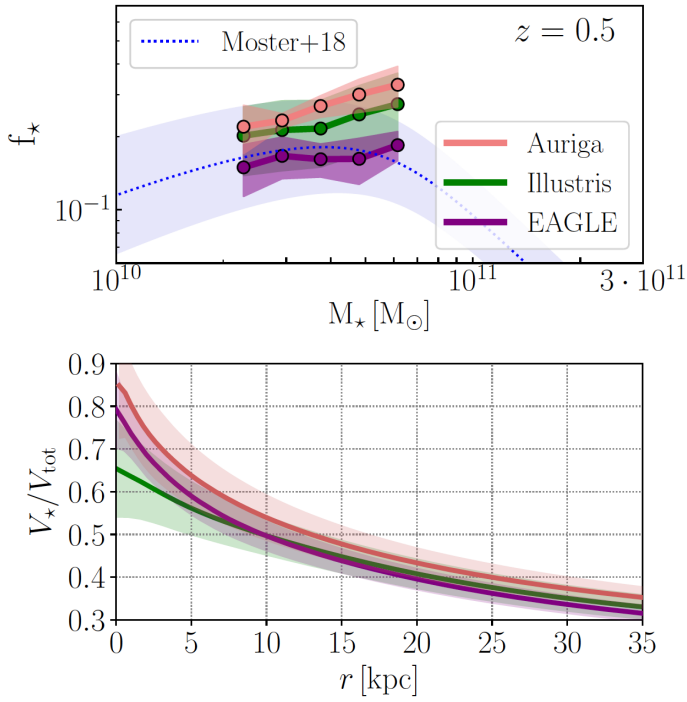


Fig. C.1. Stellar to dark matter ratios at higher redshifts: *Top:* f_* vs. M_* for Auriga, EAGLE and Illustris disc galaxies at $z = 0.5$. The dotted blue line denotes the relation determined using the Moster et al. (2018) abundance matching relation and the shaded region denotes the 1σ scatter around the relation. *Bottom* V_*/V_{tot} for the galaxies shown in the top panel. Auriga is locally more baryon-dominated than EAGLE and Illustris already at higher redshifts.